Simultaneous measurement of erythrocyte deformability and blood viscoelasticity using micropillars and co-flowing streams under pulsatile blood flows

Yang Jun Kang[a)]
Department of Mechanical Engineering, Chosun University, Gwangju, South Korea

(Received 1 September 2016; accepted 28 December 2016; published online 6 January 2017)

The biophysical properties of blood provide useful information on the variation in hematological disorders or diseases. In this study, a simultaneous measurement method of RBC (Red Blood Cell) deformability and blood viscoelasticity is proposed by evaluating hemodynamic variations through micropillars and co-flowing streams under sinusoidal blood flow. A disposable microfluidic device is composed of two inlets and two outlets, two upper side channels, and two lower side channels connected to one bridge channel. First, to measure the RBC deformability, the left-lower side channel has a deformability assessment chamber (DAC) with narrow-sized micropillars. Second, to evaluate the blood viscoelasticity in co-flowing streams, a phosphate buffered saline solution is supplied at a constant flow rate. By closing or opening a pinch valve connected to the outlet of DAC, blood flows in forward or back-and-forth mode. A time-resolved micro-particle image velocimetry technique and a digital image processing technique are used to quantify the blood velocity and image intensity. Then, RBC deformability is evaluated by quantifying the blood volume passing through the DAC under forward flow, and quantifying the variations of blood velocity and image intensity in the DAC under back-and-forth flow. Using a discrete circuit model, blood viscoelasticity is obtained by evaluating variations of blood velocity and co-flowing streams. The effect of several factors (period, hematocrit, and base solution) on the performance is quantitatively evaluated. Based on the experimental results, the period of sinusoidal flow and hematocrit are fixed at 30 s and 50%, respectively. As a performance demonstration, the proposed method is employed to detect the homogeneous and heterogeneous blood composed of normal RBCs and hardened RBCs. These experimental results show that the RBC deformability is more effective to detect minor subpopulations of heterogeneous bloods, compared with blood viscoelasticity. Therefore, it leads to the conclusion that the proposed method has the ability to evaluate RBC deformability and blood viscoelasticity under sinusoidal blood flow, with sufficient accuracy and high-throughput. *Published by AIP Publishing.* [http://dx.doi.org/10.1063/1.4973863]

I. INTRODUCTION

Among the various components of blood, red blood cells (RBCs) have a strong relation to the biophysical properties of blood as RBCs constitute approximately 45% of the blood volume. The biophysical properties of blood, such as shearing viscosity, viscoelasticity, RBC aggregation, and RBC deformability,[1–3] could provide valuable information on the variations in hematological disorders or diseases.[4–8] Among them, RBC deformability plays an essential role in gas transport and flow regulation.[9] In other words, owing to its high flexibility, individual RBC can pass through extremely narrow-sized capillary or endothelial slits in the spleen.[10] However,

[a)]Electronic mail: yjkang2011@chosun.ac.kr. Fax: +82-62-230-7055.

a decrease in the RBC deformability contributes to inducing microvascular occlusion and impaired perfusion of the peripheral tissues. Therefore, the RBC deformability has been considered as a promising biomarker for early detection of hematological diseases.

Recently, as microfluidic devices offer many significant advantages over conventional techniques,[8] microfluidic-based techniques have been proposed to quantify the RBC deformability.[11] First, by precisely manipulating a syringe pump or pressure source, individual RBC passes through a microfluidic channel sequentially. Then, the deformability of individual RBC is evaluated by monitoring the dynamic behaviors of single RBC by means of several parameters such as the RBC velocity,[10,12] electrical impedance,[13,14] membrane tension,[15] and morphology variations.[16,17] The single RBC-based approach is effective for studying the variations in individual RBCs, with high sensitivity. However, this method does not provide a high throughput because it requires precise manipulation of individual RBC in a microfluidic device. Second, after delivering the diluted blood (Hematocrit $[H_{ct}] = 1\%–5\%$) into a microfluidic device with micropillars during a specific duration, RBC deformability is quantified by counting the number of RBCs trapped in the channel.[18,19] This population-based approach can provide high throughput, compared to the single RBC-based approach. However, this method still requires the dilution procedure and fails to provide the dynamic behaviors of RBCs. To resolve these issues, our group suggests a simple method to evaluate the RBC deformability of blood sample with a high value of hematocrit ($H_{ct} = 50\%$). While the blood is delivered into micropillars under a constant flow rate, the deformability of RBCs is evaluated by analyzing the temporal variations of blood velocity or image intensity for a specific duration.[20,21] The previous method could provide high throughput and precise detection of minor differences in subpopulations. However, the previous method is applied to quantify the RBC deformability and blood viscosity, especially under a constant blood flow condition. For example, when monitoring the biophysical property of blood circulating within the ex-vivo or in-vitro closed fluidic circuit, blood was periodically flowed with a pulsatile pump. Under dynamic blood flows, the quantification parameter and device operation method should be newly updated. In other words, since RBCs are exposed to pulsatile blood flow, the previous method still has technical limitations on the measurement of RBC deformability under pulsatile blood flows. Simultaneously, blood viscoelasticity measurement should be newly devised to quantify variations of blood rheological properties under pulsatile blood flows.

In this study, a simple measurement technique of RBC deformability and blood viscoelasticity is suggested by evaluating the oscillation of blood flow through micropillars, and quantifying co-flowing streams in a microfluidic device. A microfluidic analogue of a Wheatstone-bridge circuit is designed for demonstrating the proposed method. First, to measure the RBC deformability with high throughput, the microfluidic device has a deformability assessment chamber (DAC) with narrow-sized micropillars. To induce pulsatile blood flow in the microfluidic device, the blood sample is supplied at a sinusoidal flow rate by operating a precise syringe pump. After closing a pinch valve connected to the outlet of the DAC, back-and-forth blood flow occurs through the micropillars. Then, the deformability of the RBCs is quantified by analyzing the temporal variations of blood velocity and image intensity in the DAC. Second, blood viscoelasticity is obtained by evaluating the temporal variations of blood velocity and co-flowing streams.

Compared to previous methods, the proposed method has several distinct advantages. First, the deformability of RBCs can be measured by quantifying forward and back-and-forth blood flows through micropillars, under pulsatile blood flows. Second, the proposed method has the ability to simultaneously measure the RBC deformability and blood viscoelasticity. In other words, blood viscoelasticity is employed to effectively monitor variations of blood rheological properties under pulsatile blood flows. Third, the proposed method can be used for precisely detecting minor subpopulations of heterogeneous blood, with accuracy. At last, the suggested method can evaluate the variations of blood biophysical properties in a label-free and high throughput fashion (i.e., hematocrit = 50%, blood volume = 0.3 ml, and test time = 20 min).

The feasibility of the proposed method is evaluated by developing a simple mathematical model and conducting experimental tests. Under sinusoidal blood flow, the effect of various

factors (period, hematocrit, and base solution) on the performance is quantitatively evaluated. A simple mathematical model is developed by using discrete fluid elements including resistances and compliances. Blood viscoelasticity is evaluated with the simple model. As a performance demonstration, the proposed method is employed to evaluate the homogeneous blood composed of RBCs that are fixed with the same concentration of glutaraldehyde (GA) solution. Thereafter, the proposed method is used to detect the minor subpopulations of heterogeneous blood prepared by partially mixing the normal RBCs and hardened RBCs.

II. METHODS AND MATERIALS

A. The proposed method for quantification of erythrocyte deformability

The measurement technique for evaluating RBC deformability and blood viscoelasticity is proposed by quantifying the temporal variations of forward and back-and-forth flows, and monitoring co-flowing streams, under pulsatile blood flows. Figure 1(A-a) shows a schematic of the

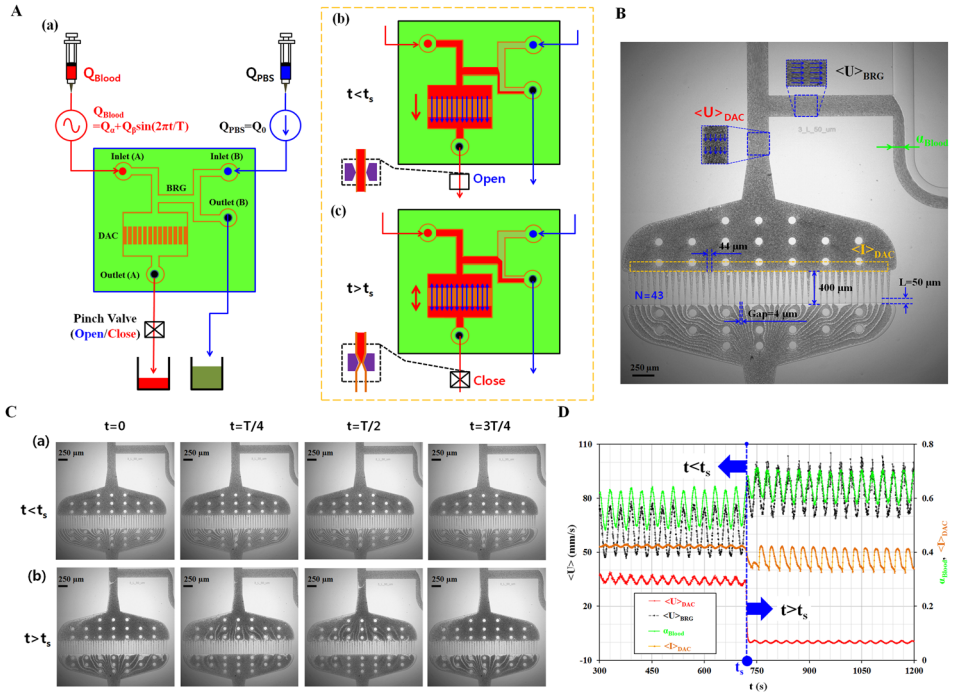

FIG. 1. Proposed method for quantification of the RBC deformability and blood viscoelasticity under pulsatile blood flows. (A) Schematic diagram of the proposed method including a disposable microfluidic device and two syringe pumps. (a) The microfluidic device has two inlets (A, B) and two outlets (A, B), two upper side channels, and two lower side channels connected to one bridge channel (BRG). To measure the deformability of RBC, the left-lower side channel has a deformability assessment chamber (DAC) with narrow-sized micropillars. Blood flow in the DAC is controlled by closing or opening a pinch valve connected to the end of outlet (A). To induce pulsatile blood flow in the microfluidic device, the blood is delivered into inlet (A) at a sinusoidal flow rate [$Q_{Blood} = Q_\alpha + Q_\beta \sin(2\pi t/T)$]. The PBS solution is supplied to inlet (B), at a constant flow-rate ($Q_{PBS} = Q_0$). (b) By opening the pinch valve (i.e., $t < t_s$), blood flows in the DAC in the forward mode. (c) By closing the pinch valve (i.e., $t > t_s$), blood flows in the DAC in the back-and-forth mode. (B) The average velocities of blood flow in the DAC ($\langle U \rangle_{DAC}$) and bridge channel ($\langle U \rangle_{BRG}$) are evaluated using a time-resolved micro-PIV technique. Using the high-speed camera that is triggered by the function generator at intervals of 0.5 s, two microscopic images are consecutively captured at a frame rate of 5 kHz. The average image intensity within a specific region of interest (ROI) in front of the micropillars ($\langle I \rangle_{DAC}$) and blood-filled width in the right-lower side channel (α_{Blood}) are quantified using digital image processing. (C) Microscopic images with respect to (a) forward mode and (b) back-and-forth mode over a period of time (t) [$t = 0$, $T/4$, $T/2$, $3/4T$]. Blood (Hematocrit [H_{ct}] = 50%) is prepared by adding normal RBCs into autologous plasma. The period is 30 s ($T = 30$ s). (D) By conducting the time-resolved micro-PIV technique and digital image processing, four parameters ($\langle U \rangle_{DAC}$, $\langle U \rangle_{BRG}$, $\langle I \rangle_{DAC}$, and α_{Blood}) are obtained for a specific duration. After closing the pinch valve at 720 s ($t_s = 720$ s), $\langle U \rangle_{DAC}$ is significantly decreased because of blood flowing in the back-and-forth mode in the DAC. The $\langle I \rangle_{DAC}$ shows large variations in amplitude. The $\langle U \rangle_{BRG}$ and α_{Blood} tend to increase, because most of the blood is passed through the bridge channel instead of the DAC.

experimental setup including a disposable microfluidic device and two syringe pumps (neMESYS, Centoni Gmbh, Germany). The microfluidic device has two inlets (A, B) and outlets (A, B), two upper side channels, and two lower side channels that are connected to one bridge channel (BRG). To measure RBC deformability by quantifying hemodynamic variations, the left-lower side channel is carefully designed to have the DAC with narrow-sized micropillars (Gap = 4 μm, depth (h) = 4 μm, length (L) = 50 μm, and N = 43) as shown in Fig. 1(B). Here, the depth and gap of each micropillar are determined by referring to previous studies.[14,18,22–25] To induce the pulsatile blood flow in the microfluidic device, a blood sample is supplied to inlet (A) at a sinusoidal flow rate [i.e., $Q_{Blood} = Q_\alpha + Q_\beta \sin(2\pi t/T)$]. Here, Q_α and Q_β denote the mean flow rate (i.e., $Q_\alpha = 1$ ml/h) and amplitude flow rate (i.e., $Q_\beta = 0.5$ ml/h), respectively. T represents the period of blood flow rate. The phosphate buffered saline (PBS) solution, as a reference fluid, is delivered into inlet (B) at a constant flow rate (i.e., $Q_{PBS} = Q_0 = 1$ ml/h). To control blood flows (i.e., forward and back-and-forth modes) in the DAC, a pinch valve is connected to the outlet (A). By opening the pinch valve for a specific duration ($t < t_s$), blood flows in the forward mode as shown in Fig. 1(A-b). After the specific duration is elapsed ($t > t_s$), blood flows in the back-and-forth mode as shown in Fig. 1(A-c).

Using the high-speed camera triggered by the function generator at intervals of 0.5 s, two microscopic images are consecutively captured at a frame rate of 5 kHz. As shown in Fig. 1(B), the average velocities of blood fields in the DAC ($\langle U \rangle_{DAC}$) and bridge channel ($\langle U \rangle_{BRG}$) are evaluated by conducting a time-resolved micro-particle image velocimetry (PIV) technique. In addition, the average values of image intensity within a specific region of interest (ROI) in front of the micropillars ($\langle I \rangle_{DAC}$) and the blood-filled width in the right-lower side channel (α_{Blood}) are quantified by conducting digital image processing.

As a preliminary study, a blood sample ($H_{ct} = 50\%$) is prepared by adding normal RBCs into autologous plasma. The period is set to 30 s (i.e., $T = 30$ s). Figures 1(C-a) and 1(C-b) show sequential microscopic images during a single period of time (t) [$t = 0$, $T/4$, $T/2$, and $3/4T$] with respect to the forward mode and back-and-forth mode. After a conducting time-resolved micro-PIV technique and digital image processing, four parameters ($\langle U \rangle_{DAC}$, $\langle U \rangle_{BRG}$, $\langle I \rangle_{DAC}$, and α_{Blood}) are obtained for a specific duration as shown in Fig. 1(D). After closing the pinch valve at 720 s (i.e., $t_s = 720$ s), $\langle U \rangle_{DAC}$ is significantly decreased. The $\langle I \rangle_{DAC}$ shows large variations in amplitude. However, the blood velocity in the BRG ($\langle U \rangle_{BRG}$) and the blood-filled width in co-flowing streams (α_{Blood}) are increased because most blood pass through the BRG.

B. Mathematical formula of blood viscoelasticity under pulsatile blood flow

To quantify the blood viscoelasticity under pulsatile blood flow, a simple analytical expression is developed with discrete fluidic elements. As shown in Fig. S1(A) (supplementary material), blood is delivered into inlet (A) at a sinusoidal flow rate [i.e., $Q_{Blood} = Q_\alpha + Q_\beta \sin(2\pi t/T)$]. PBS solution is supplied into inlet (B) at a constant flow rate (i.e., $Q_{PBS} = Q_0$). After closing a pinch valve connected to outlet (A), blood flow is changed from the forward mode to back-and-forth mode in the DAC. Thereafter, most bloods pass through the BRG. Blood and the PBS solution are formed as co-flowing streams in the lower-right side channel. Here, α_{Blood} and α_0 denote the blood-filled width and PBS-filled width, respectively. Under the sinusoidal blood flow, blood includes viscosity and elasticity. The viscoelastic effect of blood is modeled with a resistance element (R_x) and a compliance element (C_x). In addition, the viscosity effect of the PBS solution is modeled with a resistance element (R_0).

Figure S1B (supplementary material) shows the discrete fluidic model of the proposed microfluidic system. The viscoelastic effect of blood in the BRG is modeled with a resistance element (R_{BRG}) and a compliance element (C_1) combined in parallel. Blood flows in microfluidic channels are modeled with resistance elements (R_{BRG}, R_x, R_0), compliance elements (C_1, C_x), and pressures (P_m, P_n) for junction points (m, n).

First, by applying the flow-rate conservation law at the junction point (m), blood flow (Q_{Blood}) is expressed as

$$Q_{Blood} = \frac{P_m - P_n}{R_{BRG}} + C_1 \frac{d}{dt}(P_m - P_n). \tag{1}$$

Using the blood flow (Q_1) through the resistance element (R_{BRG}), the pressure drop (i.e., $\Delta P_1 = P_m - P_n$) is expressed as $\Delta P_1 = R_{BRG} \cdot Q_1$. Using the pressure drop expression, the blood flow (Q_{Blood}) is simply derived as

$$Q_{Blood} = \lambda_{BRG} \frac{d}{dt} Q_1 + Q_1. \tag{2}$$

In Eq. (2), λ_{BRG} is denoted as $\lambda_{BRG} = R_{BRG} \cdot C_1$. The resistance ($R_{BRG}$) is expressed as $R_{BRG} = 12\mu_{Blood} \cdot L_{BRG}/(W\ h^3)$. Here, L_{BRG} denotes the channel length of the bridge channel. By conducting a harmonic analysis with $Q_1 = Q_a + Q_b \sin(2\pi t/T)$, the analytical solution of the flow rate (Q_1) is analytically derived as

$$Q_1 = Q_\alpha + \frac{Q_\beta}{\sqrt{1 + {\lambda_{BRG}}^2 \cdot \left(\frac{2\pi}{T}\right)^2}} \sin\left(\frac{2\pi t}{T} - \phi\right). \tag{3}$$

In Eq. (3), the phase angle (ϕ) is given as $\phi = tan^{-1}\ (2\pi\lambda_{BRG}/T)$. Using Eq. (3), pulsation index (PI),[26] which is defined as the ratio of the difference between the maximum flow rate (Q_{max}), and the minimum flow rate (Q_{min}) to the average flow rate (Q_{ave}), is analytically derived as

$$PI = \frac{Q_\beta}{Q_\alpha} \cdot \frac{1}{\sqrt{1 + {\lambda_{BRG}}^2 \cdot \left(\frac{2\pi}{T}\right)^2}}. \tag{4}$$

Using the analytical formula of the PI, Eq. (4), the time constant (λ_{BRG}) can be evaluated by analyzing the temporal variation of blood flow in the bridge channel (i.e., $\langle U \rangle_{BRG}$) under sinusoidal blood flow.

Second, by using the flow-rate conservation law of two fluids at a junction point (n), the following equations are given as Eqs. (5) and (6)

$$Q_{Blood} = C_x \frac{d}{dt}(P_n) + \frac{P_n}{R_x}, \tag{5}$$

$$Q_{PBS} = \frac{P_n}{R_0}. \tag{6}$$

Substituting Eq. (6) into Eq. (5), the flow rate ratio of blood in relation to the PBS solution (Q_{Blood}/Q_{Ref}) is derived as Eq. (7)

$$\frac{Q_{Blood}}{Q_{PBS}} = C_x \frac{d}{dt}(R_0) + \frac{R_0}{R_x}. \tag{7}$$

In Eq. (7), the fluidic resistances of blood sample (R_x) and PBS solution (R_0) can be approximately expressed as $R_x = 12\mu_{Blood} \cdot L_x/(\alpha_{Blood} \cdot W \cdot h^3)$ and $R_0 = 12\mu_0 \cdot L_x/[(1-\alpha_{Blood}) \cdot W \cdot h^3]$ for a rectangular microfluidic channel with extremely low-aspect ratio (i.e., $h/W = 4/250$). When the resistances (R_x and R_0) are substituted into Eq. (7), the first order differential equation is derived as Eq. (8)

$$\lambda_{sc} \frac{d}{dt}\left(\frac{1}{1 - \alpha_{Blood}}\right) + \left(\frac{1}{1 - \alpha_{Blood}}\right) = \left(\frac{Q_{Blood}}{Q_{PBS}}\right)\left(\frac{\mu_{Blood}}{\mu_0}\right) + 1. \tag{8}$$

In Eq. (8), the time constant (λ_{SC}) is expressed as $\lambda_{SC} = C_x \cdot R_{BRG} \cdot L_x / L_{BRG}$. Here, L_x denotes the channel length of the right-lower side channel. For a simple derivation procedure, it is assumed that blood viscosity remained constant without respect to blood-filled width (α_{Blood}).[27] In addition, the time constants (λ_{BRG}, λ_{SC}) have a linear relationship (i.e., $\lambda_{SC} = a_1 \lambda_{BRG} + a_2$). After integrating both sides of Eq. (8) for a single period (T) and re-arranging it, the formula of blood viscosity (μ_{Blood}) is given as

$$\mu_{Blood} = \left(\frac{\mu_0}{T}\right)\left(\frac{Q_0}{Q_\alpha}\right)\left[\lambda_{SC}\int_0^T \frac{d}{dt}\left(\frac{1}{1-\alpha_{Blood}}\right)dt + \int_0^T \frac{dt}{1-\alpha_{Blood}} - T\right]. \quad (9)$$

After estimating λ_{BRG} from Eq. (4), λ_{SC} is estimated from the linear relationship evaluated through experimental procedures. Blood viscosity (μ_{Blood}) is evaluated by inserting λ_{SC} into Eq. (9). Thereafter, the elasticity of blood (G_{Blood}) is estimated from the time constant formula of the Maxwell model (i.e., $\lambda_{SC} = \mu_{Blood}/G_{Blood}$).[28]

C. Fabrication of a microfluidic device and experimental procedure

A microfluidic device was designed to have two inlets (A, B), two outlets (A, B), and upper side channels (width $[W] = 250\,\mu$m) and right-lower side channels ($W = 250\,\mu$m) connected to one bridge channel ($W = 250\,\mu$m). To design both side channels with a low aspect ratio (i.e., $h/W \ll 1$), the channel depth was set to $4\,\mu$m (i.e., $h = 4\,\mu$m). A silicon mold was fabricated using the conventional micro-electro-mechanical-system techniques including photolithography and deep reactive-ion etching (DRIE). After mixing polydimethylsiloxane (PDMS) at 10:1 ratio with a curing agent, the mixture was poured onto the silicon mold positioned in a Petri dish. The air bubbles dissolved in the PDMS were completely removed by operating a vacuum pump for 2 h. After curing the PDMS in a convection oven at a temperature of 80 °C for 2 h, the PDMS block was peeled off from the silicon mold. After treating the oxygen plasma (CUTE-MPR, Femto Science Co., South Korea) on the PDMS block and on a glass substrate simultaneously, the microfluidic device was prepared by bonding the PDMS block to the glass substrate.

The microfluidic device was mounted on an optical microscope (Olympus, Tokyo, BX51) equipped with a 4× objective lens (NA = 0.1). Two polyethylene tubes (inner diameter = 250 μm, length = 300 mm) and two polyethylene tubes (inner diameter = 250 μm, length = 100 mm) were connected to two inlets and outlets, respectively. A pinch valve was installed at the end of the polyethylene tube connected to outlet (A). To remove air bubbles in the microfluidic channel and avoid non-specific binding of plasma protein to the inner surface of the microfluidic channel, 1% Bovine Serum Albumin (BSA) diluted with 1× PBS solution (pH 7.4, GIBCO, Life Technologies, South Korea) was delivered into the microfluidic device, at a flow rate of 1 ml/h for 20 min. Thereafter, two syringes filled with the blood and PBS solution were connected to the end of the polyethylene tube connected to inlets (A, B). A high-speed camera (FASTCAM MINI, Photron, USA.) was employed for capturing the blood flows in microfluidic channels. The camera has a spatial resolution of 1280 × 1000 pixels. Each pixel corresponds to 10 μm. When a function generator (WF1944B, NF Corporation, Japan) triggered the high-speed camera at intervals of 0.5 s, two microscopic images were sequentially captured at a frame rate of 5 kHz. All experiments were conducted at a room temperature of 25 °C.

D. Quantifications of blood physical properties

First, to evaluate the temporal variations of blood flow in the DAC and BRG, velocity fields were obtained by conducting a time-resolved micro-PIV technique. Two specific ROIs (50 × 60 pixels) in the DAC and BRG were selected to obtain the velocity fields of blood flow, as shown in Fig. 1(B). The size of the interrogation window was 16 × 16 pixels. Window overlap was 50%. The obtained velocity fields were validated with a median filter. The average

velocities of blood flow in the DAC and BRG ($\langle U\rangle_{DAC}$, $\langle U\rangle_{BRG}$) were calculated as an arithmetic average over the ROI.

Second, to evaluate variations of image intensity of blood that flows in the DAC, a specific ROI (730 × 20 pixels) was selected in front of the micropillars, as shown in Fig. 1(B). The average of pixel values over the ROI ($\langle I\rangle_{DAC}$) was estimated by performing digital image processing with a commercial software (Matlab, Mathworks, USA).

Finally, a specific ROI (40 × 50 pixels) was selected for evaluating the blood-filled width (α_{Blood}) in the right-lower side channel, as shown in Fig. 1(B). Using the commercial software (Matlab, Mathworks, USA), the temporal variations of α_{Blood} were evaluated quantitatively. To detect the interfacial line between two fluids, the captured images were converted into binary images with Otsu's method. By conducting an arithmetic average of pixel values over the ROI, the blood-filled width (α_{Blood}) was obtained with an elapse of time. The viscosity of the PBS solution was assumed to be 1 ± 0.05 cP.[29]

E. Sample preparation of test fluids

To evaluate RBC deformability and blood viscoelasticity with the proposed method, various blood samples were prepared by adding human RBCs to the base solution (Plasma, 1× PBS). Concentrated RBCs and plasma were provided by the Gwangju-Chonnam Blood Bank (Gwangju, South Korea). Hematocrits of normal blood ($H_{ct} = 20\%$, 30%, 40%, and 50%) were adjusted by adding normal RBCs to the base solution (plasma, 1× PBS). Three concentrations of glutaraldehyde (GA) solution ($C_{GA} = 0.13\%$, 0.25%, and 0.38%) were diluted by adding GA solution (Grade II, 25% in H_20, Sigma-Aldrich, USA) into a 1× PBS solution. Normal RBCs were hardened after dipping the normal RBCs into the diluted GA solution for a specific duration of 10 min. Thereafter, homogeneous hardened blood samples were prepared by adding hardened RBCs to 1× PBS solution. On the other hand, heterogeneous blood mixed with hardened blood volume-fraction (i.e., $\psi = V_{Hard}/[V_{Hard} + V_{Norm}]$) ($\psi = 0\%$, 10%, 20%, and 100%) were prepared by partially adding the hardened blood into the normal blood. Here, V_{Hard} and V_{Norm} denote the hardened blood volume and the normal blood volume, respectively. The hematocrit of blood was carefully adjusted to 50%.

F. Statistical analysis

In this study, the statistical analysis was conducted with a statistical software (MINITAB, Minitab Inc., USA). T-test and ANOVA-test were applied to statistically determine the equality of two groups and the difference among group means. For all tests, if the P-value is less than 0.05, the result is considered as significant within the 95% confidence interval. The number of data is determined by the forward mode and back-and-forth mode. For the forward mode, the number of data is one. But, the back-and-forth mode changes the number of data depending on the period. For example, at the period of 30 s (i.e., $T = 30$ s), the number of data is largely over 10 (i.e., $N > 10$). On the other hand, at least three samples were used to evaluate the performance of the proposed method.

III. RESULTS AND DISCUSSION

A. Quantitative comparison between time constants obtained by blood velocity and co-flowing streams

A linear relationship (i.e., $\lambda_{SC} = a_1\lambda_{BRG} + a_2$) between time constants (λ_{BRG}, λ_{SC}) was verified by analyzing the blood flow in the bridge channel ($\langle U\rangle_{BRG}$) and the blood-filled width (α_{Blood}) with an elapse of time. Here, the normal blood ($H_{ct} = 50\%$) was prepared by adding normal RBCs into base solution (1× PBS, Plasma). To evaluate the time constants under transient blood flow, the normal blood was delivered into inlet (A) at a periodic pulse-shaped flow rate (i.e., $Q_{max} = 1$ ml/h, $Q_{min} = 0$, $T =$ period). PBS solution was supplied into inlet (B), at a constant flow rate of 1 ml/h (i.e., $Q_{PBS} = 1$ ml/h).

Figure S2(A-a) (supplementary material) shows the temporal variations of $\langle U\rangle_{BRG}$ and α_{Blood} for the normal blood (RBCs in PBS suspension, $H_{ct} = 50\%$), at a period of 240 s (i.e., $T = 240$ s). The temporal variations of $\langle U\rangle_{BRG}$ and $(1-\alpha_{Blood})^{-1}$ were best fitted as $\langle U\rangle_{BRG} = a_1 \exp(-t/\lambda_1) + a_2 \exp(-t/\lambda_2)$ and $(1-\alpha_{Blood})^{-1} = b_1 \exp(-t/\lambda_1) + b_2 \exp(-t/\lambda_2)$, respectively. Two time constants (λ_1, λ_2) were obtained by conducting a regression analysis with a commercial software (Matlab, Mathworks, USA). The inset shows the temporal variations of $\langle U\rangle_{BRG}$ and $(1-\alpha_{Blood})^{-1}$ for a specific duration of 120 s. As a result, as λ_1 is much shorter than λ_2, λ_1 was only employed to evaluate the time constants of $\langle U\rangle_{BRG}$ and $(1-\alpha_{Blood})^{-1}$. As shown in Fig. S2(A-b) (supplementary material), the time constants of $\langle U\rangle_{BRG}$ and $(1-\alpha_{Blood})^{-1}$ were estimated as $\lambda_{BRG} = 5.03 \pm 0.88$ s and $\lambda_{SC} = 4.84 \pm 0.37$ s, respectively.

To evaluate the linear relationship between time constants (λ_{BRG}, λ_{SC}), the time constants were measured with respect to period (T) and base solution (Plasma, 1× PBS). Figure S2(B-a) (supplementary material) shows the time constants of the blood sample (RBCs in PBS suspension, $H_{ct} = 50\%$) when the period (T) is varied ($T = 120$ s, 180 s, and 240 s). In addition, Figure S2(B-b) (supplementary material) shows time constants of the blood sample (RBCs in Plasma suspension, $H_{ct} = 50\%$) with respect to the period (T). As shown in Fig. S2(B-c) (supplementary material), the linear relationship of the time constants (i.e., $\lambda_{BRG} = \lambda_1$ [$\langle U\rangle_{BRG}$], $\lambda_{SC} = \lambda_1$ [$(1-\alpha_{Blood})^{-1}$]) was distinctly shown by plotting the sets of experimental results. By conducting a linear regression analysis, it was shown that two time constants have a significantly linear relationship (i.e., $\lambda_{SC} = 1.96\lambda_{BRG} - 5.38$) owing to a sufficiently high value of R^2 (i.e., $R^2 = 0.92$). These results lead to the conclusion that the time constant of co-flowing streams (λ_{SC}) can be estimated from the time constant (λ_{BRG}) obtained from the blood velocity in the bridge channel (λ_{BRG}).

B. The effect of period on RBC deformability

To evaluate the effect of the period of sinusoidal blood flow on RBC deformability, the temporal variations of average velocity ($\langle U\rangle_{DAC}$) and average intensity ($\langle I\rangle_{DAC}$) in the DAC were obtained by varying the period of sinusoidal blood flow rate. Here, a blood sample ($H_{ct} = 50\%$) was prepared by adding normal RBCs into a PBS solution. Figure 2(A) shows the temporal variations of average velocity in the DAC ($\langle U\rangle_{DAC}$) with respect to period (T) ($T = 0$,

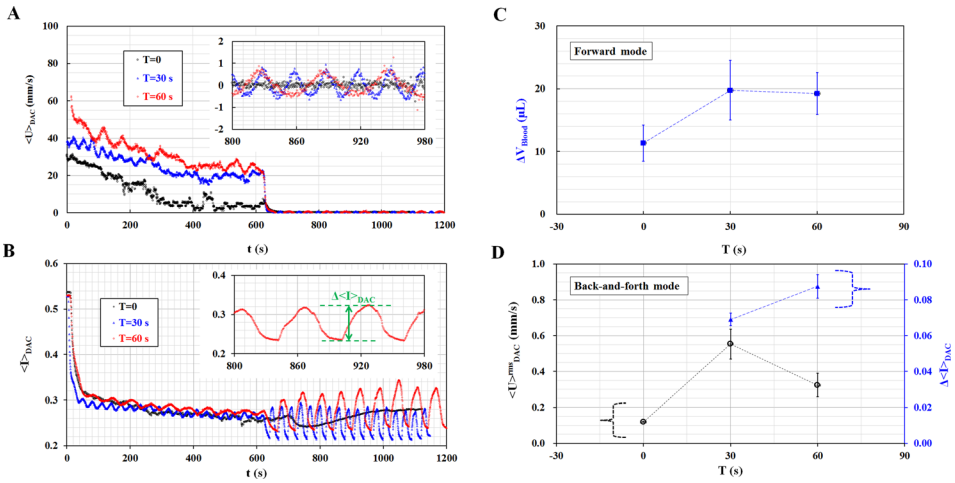

FIG. 2. Quantitative evaluations of the proposed method with a varying period of sinusoidal blood flow rate. (A) The temporal variations of blood velocity in the DAC ($\langle U\rangle_{DAC}$) with respect to period (T) of sinusoidal blood flow rate ($T = 0$, 30 s, and 60 s). The inset shows the temporal variations of $\langle U\rangle_{DAC}$ with the pinch valve closed. (B) Variations of image intensity of blood within a specific ROI ($\langle I\rangle_{DAC}$) with respect to period. The inset shows the definition of $\Delta\langle I\rangle_{DAC}$ (i.e., $\Delta\langle I\rangle_{DAC}$ = maximum value of $\langle I\rangle_{DAC}$ – minimum value of $\langle I\rangle_{DAC}$) with the pinch valve closed. (C) Variations of blood volume passing through the DAC (ΔV_{Blood}) with respect to period under forward blood flow. (D) Variations of $\langle U\rangle^{rms}_{DAC}$ and $\Delta\langle I\rangle_{DAC}$ with respect to period with the pinch valve closed. Here, the $\langle U\rangle^{rms}_{DAC}$ represents the root mean square (rms) of $\langle U\rangle_{DAC}$.

30 s, and 60 s). As a result, the $\langle U\rangle_{DAC}$ tends to increase with increasing period ranging from T = 0 to T = 60 s. In other words, RBCs might pass through the micropillars with ease, under pulsatile blood flow. After closing the pinch valve above 600 s, the blood flow was changed from forward mode to back-and-forth mode. The inset shows the temporal variations of $\langle U\rangle_{DAC}$ with the pinch valve closed (i.e., back-and-forth mode). In addition, Figure 2(B) shows the temporal variations of the average intensity of a blood sample within a specific ROI ($\langle I\rangle_{DAC}$) with varying periods. The inset shows the definition of $\Delta\langle I\rangle_{DAC}$ (i.e., $\Delta\langle I\rangle_{DAC}$ = maximum value of $\langle I\rangle_{DAC}$ − minimum value of $\langle I\rangle_{DAC}$) with the pinch valve closed.

First, under forward blood flow, the blood volume passing through the DAC (ΔV) was calculated by integrating blood velocity ($\langle U\rangle_{DAC}$) for the specific duration of 600 s (i.e., $t_s = 600$ s) with the pinch valve opened. In other words, $\Delta V = A_c \cdot \int_{t=0}^{t=t_s} \langle U\rangle_{DAC} dt$. The term A_c denotes the cross-sectional area of the rectangular microfluidic channel. Figure 2(C) shows variations of ΔV with increasing period. The result indicates that the ΔV for a sinusoidal blood flow ($T = 30$ s, and 60 s) is much larger than that of a steady blood flow ($T = 0$). In other words, taking into account the fact that the average value of flow rate is identical for steady pulsatile blood flows, the amplitude of pulsatile flow might contribute to increasing the ΔV. From this result, the blood volume (ΔV) passing through the narrow-sized micropillars is largely increased, especially under pulsatile blood flow rather than steady blood flow.

Second, under back-and-forth blood flow, $\langle U\rangle^{rms}_{DAC}$ and $\Delta\langle I\rangle_{DAC}$ were obtained with respect to the period. Here, $\langle U\rangle^{rms}_{DAC}$ was estimated using the mathematical expression: $\langle U\rangle^{rms}_{DAC} = \sqrt{\frac{1}{T}\int_{t=0}^{t=T} \langle U\rangle_{DAC}{}^2 dt}$. As shown in Fig. 2(D), the $\langle U\rangle^{rms}_{DAC}$ and $\Delta\langle I\rangle_{DAC}$ were varied depending on the period. As three parameters (ΔV, $\langle U\rangle^{rms}_{DAC}$, and $\Delta\langle I\rangle_{DAC}$) are influenced by the period, blood was delivered at a fixed period of $T = 30$ s during all following experiments.

C. The effect of hematocrit and base solution on RBC deformability and blood viscoelasticity

To verify the effect of hematocrit and base solution (1× PBS, Plasma) on the RBC deformability and blood viscoelasticity, blood with various hematocrits were prepared by adding normal RBCs into the base solution (1× PBS, Plasma). Figure 3(A-a) shows the temporal variations of $\langle U\rangle_{DAC}$ and α_{Blood} with respect to the base solution (1× PBS, Plasma) by sequentially opening and closing the pinch valve. Here, two blood samples ($H_{ct} = 50\%$) were prepared by adding normal RBCs into the PBS solution or Plasma. The inset shows the temporal variations of $\langle U\rangle_{DAC}$ with the pinch valve closed. As the viscosity of PBS solution is lower than that of the Plasma (i.e., $\mu_{PBS} < \mu_{Plasma}$), the blood flow of RBCs in a PBS suspension is higher than that of the RBCs in a Plasma suspension (i.e., $\langle U\rangle_{PBS} > \langle U\rangle_{Plasma}$). Under forward blood flow, the variations of ΔV and β were evaluated by varying hematocrit (H_{ct}) ($H_{ct} = 20\%$, 30%, 40%, and 50%). Here, β was evaluated by integrating α_{Blood} for the specific duration of $t_s = 600$ s (i.e., $\beta = \int_{t=0}^{t_s} \alpha_{Blood}\, dt$). As shown in Fig. 3(A-b), the volume of RBCs in PBS suspension (ΔV_{PBS}) is larger than the volume of RBCs in Plasma suspension (ΔV_{Plasma}) (i.e., $\Delta V_{PBS} > \Delta V_{Plasma}$). In addition, the blood-filled width of RBCs in Plasma suspension (β_{Plasma}) is larger than that of RBCs in PBS suspension (β_{PBS}) (i.e., $\beta_{Plasma} > \beta_{Plasma}$). Furthermore, β tends to increase with respect to hematocrit. However, the hematocrit does not significantly contribute to varying the ΔV. The inset shows a linear relationship between ΔV and β. According to the linear regression analysis, they both have a significantly linear relationship, because of a statistically significant value of R^2 (i.e., $R^2 = 0.69$, P-value = 0.01). This result indicates that β can be effectively employed to evaluate the RBC deformability, especially without quantification of blood velocity.

After closing the pinch valve (i.e., back-and-forth mode), the variations of $\langle U\rangle^{rms}_{DAC}$ and $\Delta\langle I\rangle_{DAC}$ were evaluated by varying the hematocrit and base solution, as shown in Figs. 3(B-a) and 3(B-b). As a result, hematocrit does not significantly contribute to changing $\langle U\rangle^{rms}_{DAC}$ (i.e., P-value = 0.651, ANOVA-test) and $\Delta\langle I\rangle_{DAC}$ (i.e., P-value = 0.516, ANOVA-test). In addition, $\langle U\rangle^{rms}_{DAC}$ of RBCs in plasma suspension is larger than that of RBCs in PBS suspension (i.e.,

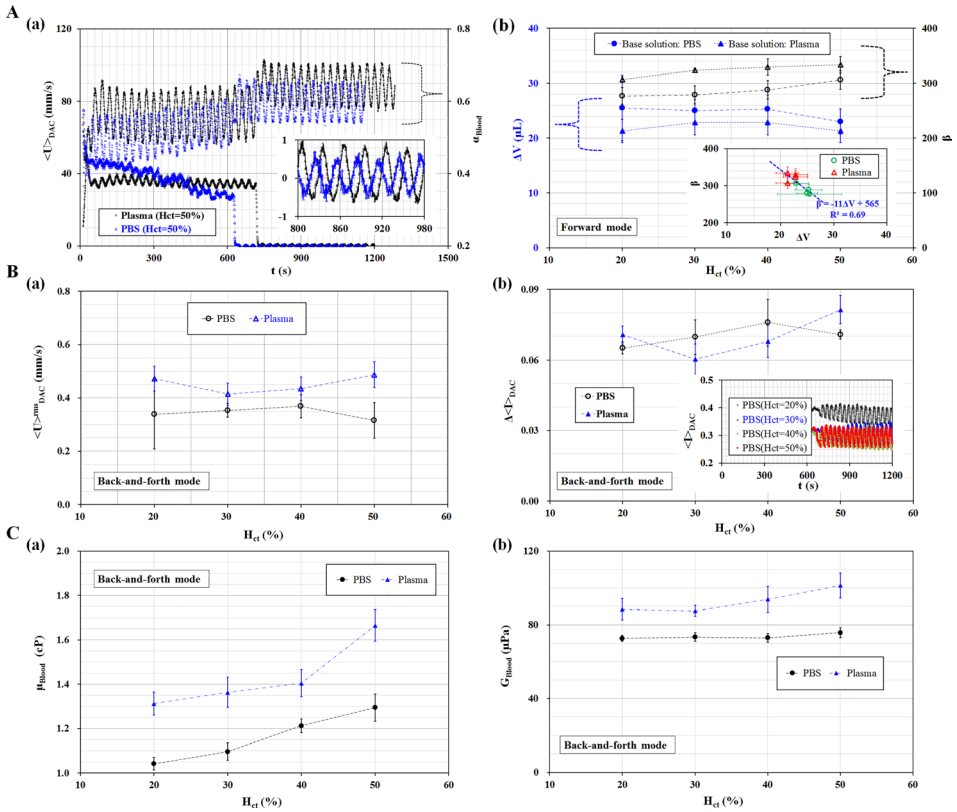

FIG. 3. Quantitative evaluation of the effect of factors, including hematocrit and base solution, on the performance of the proposed method. (A) Quantitative evaluations of $\langle U\rangle_{DAC}$ and α_{Blood} with respect to hematocrit (H_{ct}) and base solution. (a) The temporal variations of $\langle U\rangle_{DAC}$ and α_{Blood} with respect to base solution (1× PBS, Plasma) by opening and closing the pinch valve sequentially. Two blood samples ($H_{ct} = 50\%$) are prepared by adding normal RBCs into the PBS solution or Plasma. The inset shows the temporal variations of $\langle U\rangle_{DAC}$ with the pinch valve closed. (b) Variations of ΔV and β with respect to hematocrit (H_{ct}) ($H_{ct} = 20\%$, 30%, 40%, 50%). Here, β was evaluated by integrating α_{Blood} for 600 s, especially under forward blood flows. The inset shows the linear relationship between ΔV and β. (B) Quantitative evaluations of $\langle U\rangle^{rms}{}_{DAC}$ and $\Delta\langle I\rangle_{DAC}$ under back-and-forth blood flow. (a) Variations of $\langle U\rangle^{rms}{}_{DAC}$ with respect to hematocrit and base solution. (b) Variations of $\Delta\langle I\rangle_{DAC}$ with respect to hematocrit and base solution. The inset shows the temporal variations of $\langle I\rangle_{DAC}$ with respect to hematocrit of RBCs in PBS suspension. (C) Quantitative evaluation of blood viscoelasticity. (a) Variations of viscosity (μ_{Blood}) with respect to hematocrit and base solution. (b) Variations of elasticity (G_{Blood}) with respect to hematocrit and base solution.

P-value = 0.115, ANOVA-test). This result might infer that RBCs in plasma suspension have a higher deformability than RBCs in PBS suspension. Therefore, the blood velocity tends to increase at a high value of RBC deformability. In other words, the higher RBC deformability causes to decrease the fluidic resistance. In addition, $\Delta\langle I\rangle_{DAC}$ does not show significant variations with respect to hematocrit (i.e., P-value = 0.516, ANOVA-test) and base solution (i.e., P-value = 0.961, ANOVA-test). The inset of Fig. 3(B-b) shows the temporal variations of $\langle I\rangle_{DAC}$ with respect to hematocrit for RBCs in PBS suspension. From these experimental results, it leads to the conclusion that the hematocrit does not significantly contribute to changing $\langle U\rangle^{rms}{}_{DAC}$ and $\Delta\langle I\rangle_{DAC}$ under back-and-forth flow.

On the other hand, after closing the pinch valve (i.e., back-and-forth mode), most of blood injected from the syringe pump flowed through the bridge channel (BRG). Thus, the blood and PBS solution were formed as co-flowing streams in the right-lower side channel. Here, the viscosity (μ_{Blood}) and time constant (λ_{SC}) of blood flowing in the right-lower side channel were obtained using Eqs. (4) and (9). Thereafter, the blood elasticity (G_{Blood}) was calculated using the linear viscoelasticity Maxwell model (i.e., $G_{Blood} = \mu_{Blood}/\lambda_{SC}$).[27,28,30] As shown in Figs. 3(C-a) and 3(C-b), variations of viscosity (μ_{Blood}) and elasticity (G_{Blood}) were evaluated with respect to base solution and hematocrit. As a result, RBCs in Plasma suspension have a higher

value of blood viscosity compared to RBCs in PBS suspension (i.e., P-value = 0.005, ANOVA-test). Blood viscosity also tends to increase with increasing hematocrit (i.e., P-value = 0.032, ANOVA-test). On the other hand, RBCs in Plasma suspension have a higher value of blood elasticity compared to RBCs in PBS suspension (i.e., P-value = 0.005, ANOVA-test). Furthermore, the elasticity of RBCs in Plasma suspension tends to increase, especially above 30% hematocrit (i.e., $H_{ct} > 30\%$). However, the elasticity of RBCs in PBS suspension remained constant, without respect to hematocrit (i.e., P-value = 0.272, ANOVA-test). These results show a consistency in trend with respect to hematocrit compared to the previous study.[21,28] These experimental results lead to the conclusion that the proposed method has the ability to measure the RBC deformability and blood viscoelasticity under sinusoidal blood flow with sufficient accuracy.

D. Deformability and viscoelasticity of homogeneous hardened RBCs

As a performance demonstration of the proposed method, the RBC deformability and blood viscoelasticity were simultaneously evaluated by monitoring blood velocity in the DAC ($\langle U \rangle_{DAC}$), image intensity in the DAC ($\langle I \rangle_{DAC}$), and blood-filled width in co-flowing streams (α_{Blood}) with an elapse of time. Here, hardened RBCs were prepared by dipping normal RBCs into three concentrations of glutaraldehyde (GA) solution ($C_{GA} = 0.13\%$, 0.25%, and 0.38%) for a specific duration of 10 min. Here, the concentrations of GA solution were carefully determined to rigidify the flexible membrane of individual RBCs. Hardened blood ($H_{ct} = 50\%$) was prepared by adding homogeneous RBCs fixed with the same concentration of GA solution into a 1× PBS solution. Thereafter, the proposed method was employed to measure the RBC deformability for hardened blood composed of hardened RBCs. Figure 4(A) shows the temporal variations of $\langle U \rangle_{DAC}$ for blood which was prepared by adding normal RBCs or homogeneous RBCs fixed with 0.13% GA solution ($C_{GA} = 0.13\%$) into a 1× PBS solution. Before closing the pinch value at about 630 s (i.e., forward mode), the $\langle U \rangle_{DAC}$ of normal blood was much higher than that of hardened blood. In other words, as hardened RBCs continually clogged the micropillars, the $\langle U \rangle_{DAC}$ of hardened blood was decreased abruptly compared to normal blood. The inset shows the temporal variations of $\langle U \rangle_{DAC}$ with the pinch valve closed (i.e., back-and-forth mode). Here, the $\langle U \rangle_{DAC}$ of hardened blood is much smaller than that of normal blood. Figure 4(B) shows the temporal variations of $\langle I \rangle_{DAC}$ with respect to normal blood and hardened blood composed of hardened RBCs with $C_{GA} = 0.13\%$ (i.e., $C_{GA} = 0.13\%$). The inset shows the temporal variations of $\langle I \rangle_{DAC}$ with the pinch valve closed. As hardened RBCs were continually clogged in the micropillars, the $\langle I \rangle_{DAC}$ of fixed blood dramatically decreased within a short time. Thus, the $\langle I \rangle_{DAC}$ showed small variations in amplitude compared with normal blood. Figure 4(C) shows the temporal variations of $\langle U \rangle_{BRG}$ and α_{Blood} with respect to normal blood and hardened blood (i.e., $C_{GA} = 0.13\%$). As a result, the α_{Blood} of hardened blood is larger than that of normal blood. In other words, the deformability of RBC contributes to increasing blood-filled width (α_{Blood}) in co-flowing streams in the right-lower side channel.

During forward blood flow, the variations of ΔV and β were evaluated with increasing concentration of GA solution (C_{GA}) ($C_{GA} = 0\%$, 0.13%, 0.25%, and 0.38%). As shown in Fig. 4(D), the volume (ΔV) decreased with an increasing concentration of GA solution. However, β increased with an increasing concentration of GA solution. As ΔV is lower at higher concentrations of GA solution, blood flow rate increases in the right-lower side channel. Thus, the blood-filled width (α_{Blood}) and β tend to increase at higher concentrations of GA solution. The insets show the linear relationship between ΔV and β. Because the linear regression analysis provides a high value of R^2 ($R^2 = 0.91$), it is found that ΔV and β have a strongly linear relationship. Furthermore, β can be used to monitor the RBC deformability by monitoring the co-flowing streams in a microfluidic channel.

During the back-and-forth blood flow, the variations of $\langle U \rangle^{rms}_{DAC}$ and $\Delta \langle I \rangle_{DAC}$ were evaluated with increasing concentrations of GA solution. As shown in Fig. 4(E), the $\langle U \rangle^{rms}_{DAC}$ and $\Delta \langle I \rangle_{DAC}$ of hardened blood (i.e., $C_{GA} \geq 0.13\%$) was much smaller than that of normal blood. Above 0.13% concentration of GA solution (i.e., $C_{GA} > 0.13\%$), they both were remained

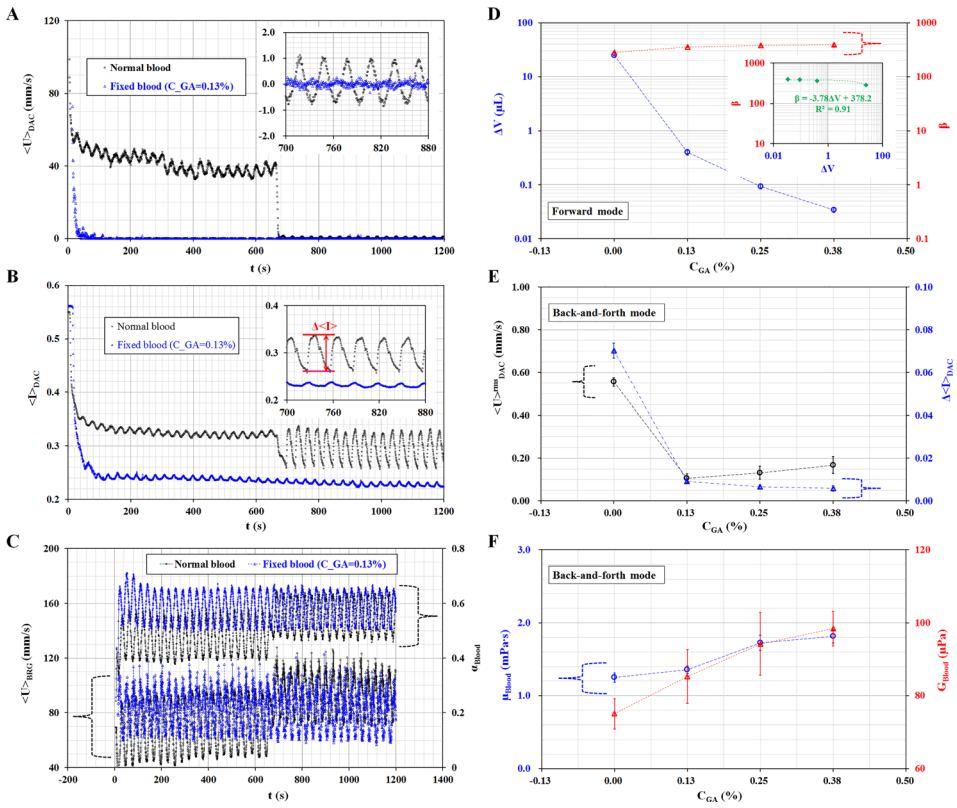

FIG. 4. Performance evaluation of the proposed method for detecting homogeneous hardened blood composed of RBCs hardened by adding glutaraldehyde (GA) solution. (A) The temporal variations of $\langle U\rangle_{DAC}$ for blood prepared by adding normal RBCs or hardened RBCs with 0.13% GA solution ($C_{GA} = 0.13\%$) into PBS solution. The inset shows the temporal variations of $\langle U\rangle_{DAC}$ with the pinch valve closed. (B) The temporal variations of $\langle I\rangle_{DAC}$ with respect to normal blood and fixed blood ($C_{GA} = 0.13\%$). The inset shows the temporal variations of $\langle I\rangle_{DAC}$ with the pinch valve closed. (C) The temporal variations of $\langle U\rangle_{BRG}$ and α_{Blood} with respect to normal blood and hardened blood ($C_{GA} = 0.13\%$). (D) Variations of ΔV and β with increasing GA concentration (C_{GA}) ($C_{GA} = 0\%$, 0.13%, 0.25%, and 0.38%) under forward blood flow. The inset shows the linear relationship between ΔV and β. (E) Variations of $\langle U\rangle^{rms}{}_{DAC}$ and $\Delta\langle I\rangle_{DAC}$ with increasing concentration of GA solution. (F) Variations of μ_{Blood} and G_{Blood} with increasing concentration of GA solution (C_{GA}).

constant. In other words, the proposed method does not provide a significant difference of hardened blood composed of RBCs fixed with GA solutions with concentrations above 0.13%.

On the other hand, to evaluate the blood rheological properties, blood viscoelasticity was measured by monitoring the temporal variations of $\langle U\rangle_{BRG}$ and α_{Blood} under the back-and-forth blood flow. Figure 4(F) shows variations of μ_{Blood} and G_{Blood} with increasing concentrations of GA solution. As expected, the blood viscosity (μ_{Blood}) tends to increase at higher concentrations of GA solution. In addition, blood elasticity (G_{Blood}) tends to increase with increasing concentrations of GA solution. This result shows a more consistent trend of blood viscoelasticity depending on the concentration of GA solution as compared to the previous study.[28]

E. Deformability and viscoelasticity of heterogeneous hardened RBCs

Finally, the proposed method was employed to detect minor subpopulations of heterogeneous blood that was prepared by partially mixing normal blood into hardened blood. Hardened blood ($H_{ct} = 50\%$) was prepared by adding RBCs fixed with 0.13% GA solution into 1× PBS solution. Normal blood ($H_{ct} = 50\%$) was also prepared by adding normal RBCs into 1× PBS solution. Hardened blood volume-fraction (ψ) is defined as the volume ratio of hardened blood in relation to the total blood volume (i.e., $\psi = V_{Hard}/[V_{Norm} + V_{Hard}]$). Figure 5(A) shows the variations of ΔV with increasing ψ ($\psi = 0\%$, 10%, 20%, and 100%), under forward blood flow.

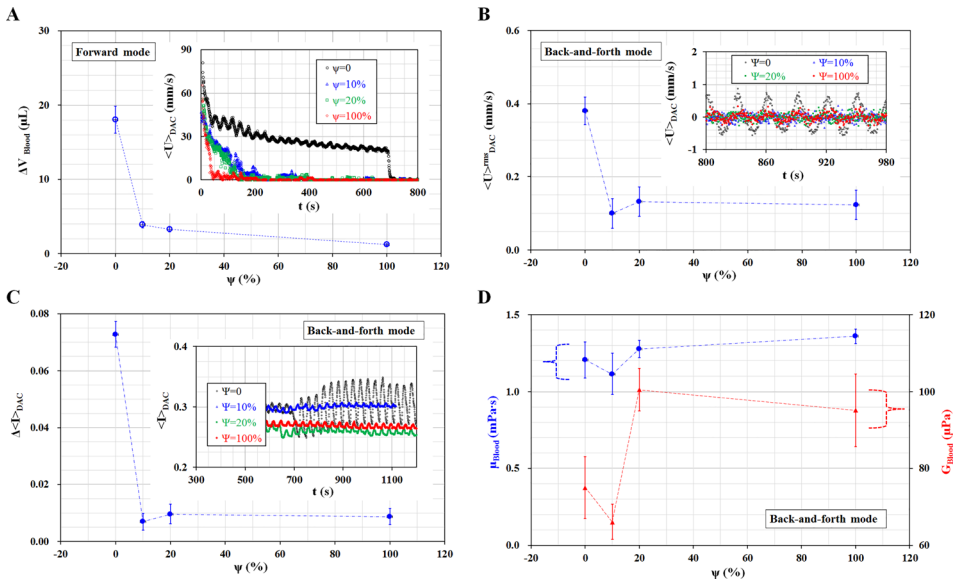

FIG. 5. Performance evaluation of the proposed method for heterogeneous hardened blood prepared by partially mixing the normal blood into hardened blood. Hardened blood is prepared by adding RBCs fixed with 0.13% GA solution into PBS solution. The hematocrit of each blood is adjusted at 50%. (A) Variations of ΔV with increasing hardened blood volume-fraction (ψ) ($\psi = 0\%$, 10%, 20%, and 100%). Here, $\psi = 0$ and $\psi = 100\%$ denote only the normal blood (V_{Norm}) and hardened blood (V_{Hard}), respectively. The inset shows the temporal variations of $\langle U \rangle_{DAC}$ with respect to hardened blood volume-fraction (ψ). (B) Variations of $\langle U \rangle^{rms}{}_{DAC}$ with respect to hardened blood volume-fraction (ψ). The inset shows the temporal variations of $\langle U \rangle_{DAC}$ with the pinch valve closed. (C) Variations of $\Delta\langle I \rangle_{DAC}$ with respect to hardened blood volume-fraction (ψ). The inset shows the temporal variations of $\langle I \rangle_{DAC}$ with respect to hardened blood volume-fraction (ψ). (D) Variations of μ_{Blood} and G_{Blood} with respect to hardened blood volume-fraction (ψ).

Here, $\psi = 0$ and $\psi = 100\%$ denote the normal blood volume (V_{Norm}) and hardened blood volume (V_{Hard}), respectively. The inset shows the temporal variations of $\langle U \rangle_{DAC}$ depending on the hardened blood volume-fraction (ψ) ($\psi = 0\%$, 10%, 20%, and 100%). As a result, the ΔV of blood with minor subpopulations of fixed RBCs ($\psi = 10\%$) decreased significantly compared to the normal blood ($\psi = 0$). This result indicates that blood volume passing through the DAC (ΔV) can be effectively employed to detect minor subpopulations of hardened RBCs. Under back-and-forth blood flow, the variations of $\langle U \rangle^{rms}{}_{DAC}$ were obtained with increasing hardened blood volume-fraction (ψ), as shown in Fig. 5(B). The inset shows the temporal variations of $\langle U \rangle_{DAC}$ with respect to ψ. From this result, the heterogeneous hardened blood with a minor subpopulation of fixed RBCs ($\psi = 10\%$) has a much lower value of blood velocity compared to normal blood ($\psi = 0$) (i.e., P-value = 0.001, T-test). Figure 5(C) shows variations of $\Delta\langle I \rangle_{DAC}$ with respect to ψ. The insets show the temporal variations of $\langle I \rangle_{DAC}$ with respect to ψ. As a result, hardened blood with a minor subpopulation of fixed RBCs ($\psi = 10\%$) has a much lower value of $\Delta\langle I \rangle_{DAC}$ compared to normal blood (i.e., P-value = 0.001, T-test). On the other hand, as shown in Fig. 5(D), variations of viscosity (μ_{Blood}) and elasticity (G_{Blood}) were obtained by varying hardened blood volume-fraction (ψ). Blood with $\psi > 20\%$ shows potential variations of viscosity (i.e., P-value = 0.325, T-test) and elasticity (i.e., P-value = 0.055, T-test) compared to normal blood. This result might infer that hemodynamic variations in the DAC (i.e., ΔV, β, $\langle U \rangle^{rms}$, ΔI) can be effectively employed to detect the minor subpopulations in heterogeneous hardened blood, compared to variations of blood viscoelasticity.

These experimental results lead to the conclusion that the proposed method has the ability to evaluate the RBC deformability by monitoring the blood velocity ($\langle U \rangle_{DAC}$) and image intensity ($\langle I \rangle_{DAC}$) in the DAC with micropillars, especially under pulsatile blood flow. At the same time, blood viscoelasticity can be evaluated by monitoring the temporal variations of co-flowing streams under pulsatile blood flow. Furthermore, the proposed method can be used for precise detection of minor subpopulations of heterogeneous blood with sufficient accuracy and high-throughput.

IV. CONCLUSION

In this study, a simple measurement technique of RBC deformability and blood viscoelasticity was proposed by evaluating the forward flow and back-and-forth flow through micropillars and co-flowing streams under sinusoidal blood flow. To demonstrate the proposed method, the microfluidic device was mimicked from an electric Wheatstone-bridge circuit. The left-lower side channel was designed to have a unique deformability assessment chamber (DAC) with narrow-sized micropillars. By closing or opening a pinch valve connected to the DAC, blood flow was significantly changed depending on the forward mode or back-and-forth mode. A time-resolved micro-PIV technique and digital image processing technique were applied to quantify the temporal variations of blood velocity ($\langle U \rangle_{DAC}$) and image intensity ($\langle I \rangle_{DAC}$) in the DAC. Then, RBC deformability was evaluated by quantifying ΔV and β under forward flow, as well as $\langle U \rangle^{rms}{}_{DAC}$ and $\Delta \langle I \rangle_{DAC}$ under back-and-forth flow. On the other hand, blood viscoelasticity was measured to monitor the temporal variations of hemorheological properties under dynamic blood flow. The effect of various factors (period, hematocrit, base solution) on the performance was evaluated by quantifying the hemodynamic variations. Then, to provide consistent experimental results, period (T) and hematocrit (H_{ct}) were fixed at $T = 30$ s and $H_{ct} = 50\%$, respectively. Finally, the proposed method was employed to detect the minor subpopulations of heterogeneous hardened blood with partially mixing normal RBCs and hardened RBCs. From these experimental results, it was found that the proposed method has the ability to evaluate the deformability of RBC and blood viscoelasticity under pulsatile blood flow. Furthermore, the proposed method could be used for precise detection of minor subpopulations of heterogeneous blood with sufficient accuracy and high-throughput. In the near future, the proposed method will be employed for evaluating potential damages of blood circulating under an *in-vitro* closed fluidic system.

SUPPLEMENTARY MATERIAL

See supplementary material for discrete fluidic circuit model of the proposed microfluidic system (Fig. S1) and quantitative comparison of time constants (λ_{BRG}, λ_{SC}) obtained using the temporal variations of blood velocity in the bridge channel ($\langle U \rangle_{BRG}$) and blood-filled width in co-flowing streams (α_{Blood}) (Fig. S2)

ACKNOWLEDGMENTS

This work was partially supported by the Basic Science Research Program through the NRF funded by the Ministry of Science, ICT, and Future Planning (NRF-2015R1C1A1A02036624) and the research fund from Chosun University in 2014.

[1]O. Linderkamp, G. B. Nash, P. Y. K. Wu, and H. J. Meiselman, Blood **67**, 1244–1250 (1986).
[2]S. Shin, Y. Ku, and M.-S. Park, J. Mech. Sci. Technol. **19**, 216–233 (2005).
[3]S. Chien, Annu. Rev. Physiol. **49**, 177–192 (1987).
[4]N. F. Zeng, J. E. Mancuso, A. M. Zivkovic, J. T. Smilowitz, and W. D. Ristenpart, PLoS One **11**, e0156070 (2016).
[5]M. Tanyeri, M. Ranka, N. Sittipolkul, and C. M. Schroeder, Lab Chip **11**, 4181–4186 (2011).
[6]C.-Y. Wu, W.-H. Liao, and Y.-C. Tung, Lab Chip **11**, 1740–1746 (2011).
[7]S. Huang, A. Undisz, M. Diez-Silva, H. Bow, M. Dao, and J. Han, Integr. Biol. **5**, 414–422 (2013).
[8]R. Agrawal, T. Smart, J. Nobre-Cardoso, C. Richards, R. Bhatnagar, A. Tufail, D. Shima, P. H. Jones, and C. Pavesio, Sci. Rep. **6**, 15873 (2016).
[9]A. S. Popel and P. C. Johnson, Annu. Rev. Fluid Mech. **37**, 43–69 (2005).
[10]L. Liu, S. Huang, X. Xu, and J. Han, Sci. Rep. **6**, 22929 (2016).
[11]G. Tomaiuolo, Biomicrofluidics **8**, 051501 (2014).
[12]H. Bow, I. V. Pivkin, M. Diez-Silva, S. J. Goldfless, M. Dao, J. C. Niles, S. Sureshb, and J. Han, Lab Chip **11**, 1065–1073 (2011).
[13]A. Adamo, A. Sharei, L. Adamo, B. Lee, S. Mao, and K. F. Jensen, Anal. Chem. **84**, 6438–6443 (2012).
[14]Y. Zheng, E. S. Baghini, A. Azad, C. Wang, and Y. Sun, Lab Chip **12**, 2560–2567 (2012).
[15]Q. Guo, S. Park, and H. Ma, Lab Chip **12**, 2687–2695 (2012).
[16]G. Tomaiuolo, M. Barra, V. Preziosi, A. Cassinese, B. Rotoli, and S. Guido, Lab Chip **11**, 449–454 (2011).
[17]S. Sakuma, K. Kuroda, C.-H. D. Tsai, W. Fukui, F. Arai, and M. Kaneko, Lab Chip **14**, 1135–1141 (2014).
[18]S. S. Shevkoplyas, T. Yoshida, S. C. Gifford, and M. W. Bitensky, Lab Chip **6**, 914–920 (2006).
[19]P. Preira, V. Grandne, J.-M. Forel, S. Gabriele, M. Camaraa, and O. Theodoly, Lab Chip **13**, 161–170 (2013).

[20]Y. J. Kang, Y.-R. Ha, and S.-J. Lee, Anal. Chem. **88**, 2912–2922 (2016).
[21]Y. J. Kang, Y.-R. Ha, and S.-J. Lee, Analyst **141**, 319–330 (2016).
[22]J. P. Shelby, J. White, K. Ganesan, P. K. Rathod, and D. T. Chiu, Proc. Natl. Acad. Sci. U.S.A. **100**, 14618–14522 (2003).
[23]S. Youn, D. W. Lee, and Y.-H. Cho, J. Microelectromech. Syst. **17**, 302–308 (2008).
[24]Y.-C. Chen, G.-Y. Chen, Y.-C. Lin, and G.-J. Wang, Microfluid. Nanofluid. **9**, 585–591 (2010).
[25]J. P. Beech, S. H. Holm, K. Adolfssona, and J. O. Tegenfeldt, Lab Chip **12**, 1048–1051 (2012).
[26]Y. J. Kang and S. Yang, Lab Chip **12**, 1881–1889 (2012).
[27]Y. J. Kang, Analyst **141**, 6583–6597 (2016).
[28]Y. J. Kang and S.-J. Lee, Biomicrofluidics **7**, 054122 (2013).
[29]Y. J. Kang, J. Ryu, and S.-J. Lee, Biomicrofluidics **7**, 044106 (2013).
[30]J. A. Long, A. Undar, K. B. Manning, and S. Deutsch, ASAIO J. **51**, 563–566 (2005).